Atomic Force Microscopy of Biological Membranes

Patrick L. T. M. Frederix,[†] Patrick D. Bosshart,[†] and Andreas Engel[†‡*]
[†]M. E. Müller Institute for Structural Biology, Biozentrum, University of Basel, Basel, Switzerland; and [‡]Department of Pharmacology, Case Western Reserve University, Cleveland, Ohio, USA

ABSTRACT   Atomic force microscopy (AFM) is an ideal method to study the surface topography of biological membranes. It allows membranes that are adsorbed to flat solid supports to be raster-scanned in physiological solutions with an atomically sharp tip. Therefore, AFM is capable of observing biological molecular machines at work. In addition, the tip can be tethered to the end of a single membrane protein, and forces acting on the tip upon its retraction indicate barriers that occur during the process of protein unfolding. Here we discuss the fundamental limitations of AFM determined by the properties of cantilevers, present aspects of sample preparation, and review results achieved on reconstituted and native biological membranes.

INTRODUCTION

About three decades ago few would have believed that a single atom could be visualized simply by touching it. The groundbreaking study by Binnig, Gerber and Quate in 1986 laid the foundation for such an almost unbelievable possibility (1). Another milestone came soon afterward from the Hansma group that demonstrated the possibility to image proteins in their aqueous environment, thus opening an exciting avenue for structural biologists (2). This progress stimulated early work on a native biological membrane, the gap junction (3). The resolution of the method is determined by the size of the probe that touches the surface—ultimately it is the atom at the tip apex. However, as sharp as a tip that raster scans over an object may be, it cannot be expected to contour deep and narrow crevasses properly. Thus, rather flat objects like biological membranes packed with proteins that protrude only by a few nm are quite amenable to high-resolution imaging by a scanning tip. Native and reconstituted membranes densely packed with proteins embedded in the lipid bilayer have given the most beautiful results, depicting the surface structure of single membrane proteins with a lateral resolution of 0.5 nm, and a vertical one that is even better (4–9). This review summarizes the essential features of an atomic force microscope (AFM) operated in solution, with an emphasis on the fundamental limitations of the essential components. The preparation methods for membrane samples and the way to acquire high-resolution images are discussed as well. We illustrate these points with examples that have given particular new insights.

Instrumentation for high-resolution AFM imaging

The pertinent items dictating the performance of an AFM are tip, cantilever, deflection detector, piezo elements, fluid cell, and the electronic control system. Previously the tip was subject to attempts making it sharper, more reproducible,

and more robust. However, even the best tip will inevitably change upon interaction with the sample. Therefore, it is up to the experience and skill of the operator to judge the performance of the tip and to collect data when the tip is devoid of contaminants.

Whereas the tip apex dominates the lateral resolution of an AFM, the vertical detection is ultimately limited by thermal fluctuations of the cantilever. Therefore, the force exerted on the tip by thermal fluctuations F_{th} dictates the minimally measurable force F_{min}. The amplitude of thermal fluctuations can be estimated by treating the cantilever as a damped, simple harmonic oscillator (10,11). According to the equipartition theorem, the energy per oscillation mode is equal to $1/2\ k_BT$. From this and assuming that the cantilever is activated by white noise, F_{th} can be estimated (11):

$$F_{min} \ \geq \ F_{th} \ = \ \sqrt{\frac{4\ k_BT\ B}{2\pi}\frac{k_L}{f_0 \cdot Q}}. \qquad (1)$$

Here, B is the frequency bandwidth of the experiment, k_L is the spring constant and f_0 is the resonance frequency of the cantilever. Q is the quality factor of the oscillator, i.e., the ratio of stored energy, $2\pi W_0$, and friction loss per oscillation cycle, ΔW. Even with simplified models (e.g. neglecting cantilever damping close to a surface) it is instructive to calculate the properties of typical cantilevers when operated in water (Table 1). Stiffer cantilevers exhibit a higher resonance frequency f_0 as well as higher Q than softer ones, yet the thermal noise level is smaller for soft cantilevers. Intuitively one expects narrow cantilevers to exhibit a lower Q in solution than wider cantilevers but, as a result of a higher f_0, friction losses increase and Q values decrease. For oscillation mode AFM, a reasonable compromise is a cantilever with a spring constant ~10 N/m, a length between 20–100 μm, and a width of 10–20 μm (Table 1). This compromise also provides higher resonance frequencies allowing samples to be scanned at higher speed than with softer cantilevers. However, sensitive and robust deflection detectors are

TABLE 1 Properties of typical cantilevers in vacuum and in liquid

k_L	0.1				1				10				100			
l	20		100		20		100		20		100		20		100	
w	5	10	10	20	5	10	10	20	5	10	10	20	5	10	10	20
t	0.15	0.12	0.60	0.48	0.33	0.26	1.23	1.02	0.70	0.56	2.78	2.21	1.51	1.20	5.98	4.75
f_{OV}	550	437	87	69	1184	940	188	149	2553	2021	404	321	5488	4355	871	692
f_{Ol}	104	58	22	13	369	203	77	44	1198	670	240	142	3505	2076	658	418
Q	1.5	1.9	1.5	1.9	2.5	3.1	2.5	3.1	4.3	5.1	4.8	5.3	8.5	9.2	10.6	10.2
FTN	41.2	48.6	89.3	105.5	54	65	116	140	71	87	151	187	94	117	194	248
z_{th}	412	486	893	1055	54	65	116	140	7.1	8.7	15.1	18.7	0.9	1.2	1.9	2.5

k_L: spring constant (N/m).

l, w, t: cantilever length, width and thickness (in μm).

f_{OV} and f_{Ol}: resonance frequency in vacuum and water, resp. in kHz (according to Sader (10)).

Q: quality factor in water (according to Sader (10)).

$FTN = F_{th}/B^{1/2}$: force thermal noise limit in fN Hz$^{-1/2}$, derived from Eq. 1.

z_{th}: metric thermal noise limit $= FTN/k_L$ in fm Hz$^{-1/2}$.

a necessity, because the average cantilever amplitude, $z_{th} = F_{th}/k_L$, induced by the thermal fluctuations F_{th} is reduced for stiffer cantilevers and the deflection sensor rather than the Brownian motion of the cantilever may dictate the detection limit.

The optical beam deflection method has reached a high sensitivity (12) for measuring deflections and is most robust and easily adjustable. Therefore, such deflection systems are used in many commercial instruments. An even higher sensitivity is obtained by a Fabry-Perot type sensor, in which an optical cavity formed by the reflecting cantilever and a confocal mirror enhances the deflection signal by an order of magnitude (13,14) (Fig. 1).

The AFM can be operated in several imaging modes that seek to minimize variations in the tip-sample interaction. In

contact mode, the vertical deflection signal is the servo loop input for maintaining a constant deflection by a vertical displacement of sample or cantilever. Both the servo input and output can produce AFM images. The deflection signal is mainly used to visualize topographical features in images with large height differences, such as overview images. Because it is a differential signal, edges are enhanced allowing membrane patches to be easily identified. The servo output yields the quantitative height image of the sample. Most high-resolution images on membrane proteins to date have been recorded in contact mode. For measurement of proteins that are not stably packed in a lipid membrane, lateral forces acting between tip and sample in contact mode can limit the best obtainable resolution. In oscillation type AFM the cantilever is only intermittently in contact
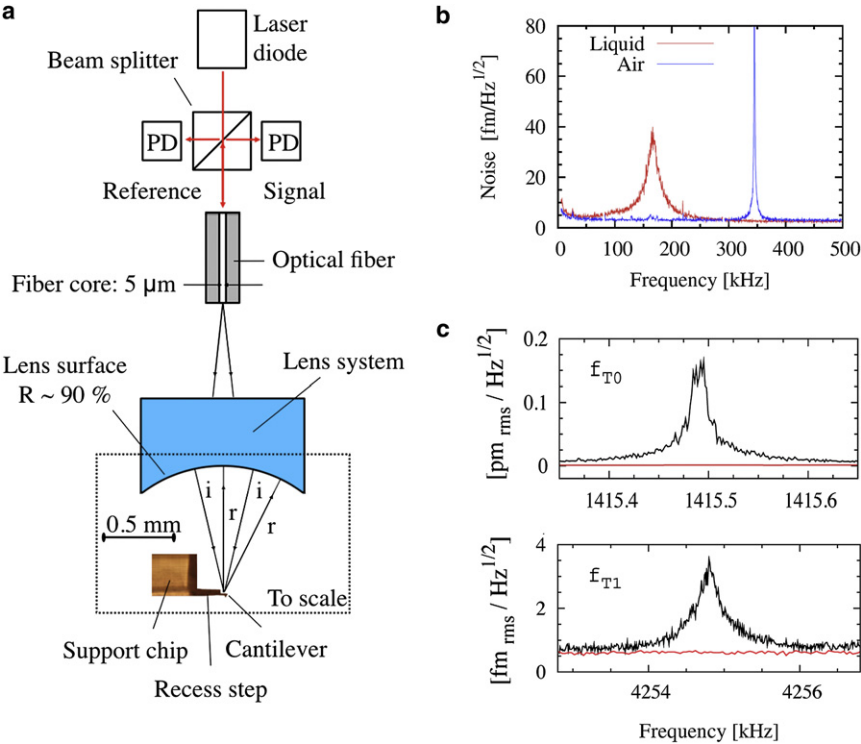
FIGURE 1 Fabry-Perot interferometer for the deflection measurement of micrometer-sized cantilevers. (a) Schematic diagram of the optical setup. Optical fiber and lens system with spherical output surface are mounted in a piezo-driven holder. (b) Thermal noise of a $k = 10^2$ N/m silicon cantilever (NCH, NanoAndMore GmbH, Wetzlar, Germany) with a gold coating at the cantilever end, in air and in water. The noise floor is <5 fm/$\sqrt{Hz}$ over a frequency band of 1–500 kHz. The damping of the cantilever oscillation by water and concomitant reduction of the resonance frequency f_0 is evident. (c) Above 1 MHz the noise floor is <1 fm/$\sqrt{Hz}$. Thermally activated torsional modes of a $223 \times 31 \times 6.7$ μm^3 silicon cantilever (NCL, NanoAndMore GmbH) with a gold coating at the cantilever end were measured in vacuum, after positioning the interferometer close to the cantilever side edge (*black curves*). To demonstrate the low noise of the deflection sensor the interferometer was centered at the end of the cantilever (*red curves*).

with the sample, thus reducing lateral forces. The servo loop in oscillation mode AFM uses the amplitude, phase or frequency change for feedback. The cantilever oscillation amplitude is a robust feedback input (15), but the phase response is faster (16). In frequency-modulation (FM)-AFM, the frequency shift can be measured as the output of a phase-locked loop that keeps the phase constant at $-\pi/2$ by adjusting the oscillation frequency. The frequency shift is then used as input for the servo loop operating the z-piezo. An advantage of FM is that the frequency shift gives quantitative information on the force acting between tip and sample (17, 18). When running the FM-AFM with small amplitudes (≤ 1 nm), a stable and quantitative operation was achieved (18, 19). The strength of FM-AFM compared to contact mode AFM was demonstrated on the voltage dependent anion channel (VDAC) in native membranes of potato mitochondrial membranes (20). Whereas in contact mode small oligomers were hard to observe and single VDAC channels were not found, monomers, dimers, trimers, tetramers and hexamers were unambiguously identified in FM-AFM.

A problem with oscillation mode AFM in liquid is the low quality factor Q of a cantilever in liquid (Table 1). Q can be pushed toward 10 by using stiff cantilevers (~ 40–$100\ \text{N m}^{-1}$). Alternatively, by the so-called Q-control technique the quality factor Q can be increased by orders of magnitude by adding a 90 degrees phase shifted oscillation source to the original oscillation (21). This gives a cleaner oscillation peak that is easier to track by the feedback loop. However, this requires reduction of the scan speed. It is still debated whether the image quality is significantly improved compared to conventional feedback by tuning other scan parameters (15), or by scanning with small amplitudes and stiff cantilevers (16,18). The low quality factor in liquid gives also rise to nonclean excitation spectra when exciting the cantilever via its chip or the complete cantilever holder. As result of the liquid coupling, system resonances of the AFM are superposed on the cantilever spectrum. A cleaner way of excitation is directly at the cantilever (e.g. magnetically) using an oscillating magnetic field and a magnetically coated cantilever, or a cantilever with magnetic particle at the free standing end (22). Unfortunately this approach is incompatible with the need for small cantilevers.

In oscillation mode AFM the height, amplitude and phase signals can be used to produce images revealing different contrast. With amplitude feedback, the phase signal is sensitive to material properties of the sample such as its visco-elasticity. Higher harmonic oscillations allow visco-elastic properties to be measured more quantitatively. These higher modes are excited during tapping at the lowest resonance frequency (23). Higher flexural harmonics are more effectively activated on cantilevers with a tip positioned off-axis. Therefore, such tips provide higher sensitivity for assessing visco-elastic properties of a sample (24). Appropriate

signal processing electronics capable of observing the signal at the tapping frequency and at the higher harmonic or lateral mode frequency is required.

A limitation of current commercial AFMs is their maximum scan speed. Several groups have worked toward increasing the imaging rate for capturing multiple frames/s while a weak tip-sample interaction force was being maintained (25–27). Major limitations for fast scanning concern the mechanical properties of the cantilever (Table 1), the z-piezo, as well as the pertinent control electronics. Nevertheless, fast vertical piezo driven displacements are possible and even in liquid stiff cantilevers exhibit sufficiently high resonance frequencies to achieve fast imaging for monitoring the dynamics of biomacromolecules (28). Fast and accurate regulation of the cantilever deflection is required to maintain a constant interaction between tip and sample, as needed to prevent force induced conformational changes (29, 30) or damage of the sample (7). Using special scanner design (27) and feedback electronics multiple image frames can now be recorded in <1 s, with subnanometer lateral resolution.

Many different piezo systems are available to laterally displace the cantilever or the sample or both—advanced scanners being controlled by a closed-loop electronics that warrants a linear and reproducible sample displacement over large distances. The latter feature is important for combining an optical microscope with an AFM for efficiently finding the area of interest identified optically, or for executing time-lapse experiments. To achieve optimum performance, the design of the fluid cell is critical as well, because it must not impair the quality of the optical path of the deflection detector, it should not couple external vibrations to the cantilever, and it should be easy to use and keep clean. Commercial AFMs optimized for biological applications offer such fluid cells.

Instrumentation for scanning electrochemical microscopy

Because AFM enables imaging of samples immersed in a physiological environment, it is possible to visualize proteins at work (28,31), i.e., observe the same proteins in different conformations induced by environmental changes. Conformational changes can be induced by force (32), pH (33,34), addition of ligands (35), applying a voltage (33), addition of ATP (36), or by light (37). To apply such stimuli locally, multifunctional cantilevers are of great interest. Examples are cantilevered scanning near field optical microscopy probes (38), pipette probes (39) or conductive probes, which are used as electrochemical sensors for instrumentation for scanning electrochemical microscopy (SECM).

Conductive cantilevers, which feature a small conductive electrode at (Fig. 2, a–b) or slightly recessed from the tip apex, have made electrochemical experiments at the nanoscale possible (40,41). Combined AFM-SECM experiments have allowed topographical features to be correlated with enzyme activity using either conical or recessed electrodes
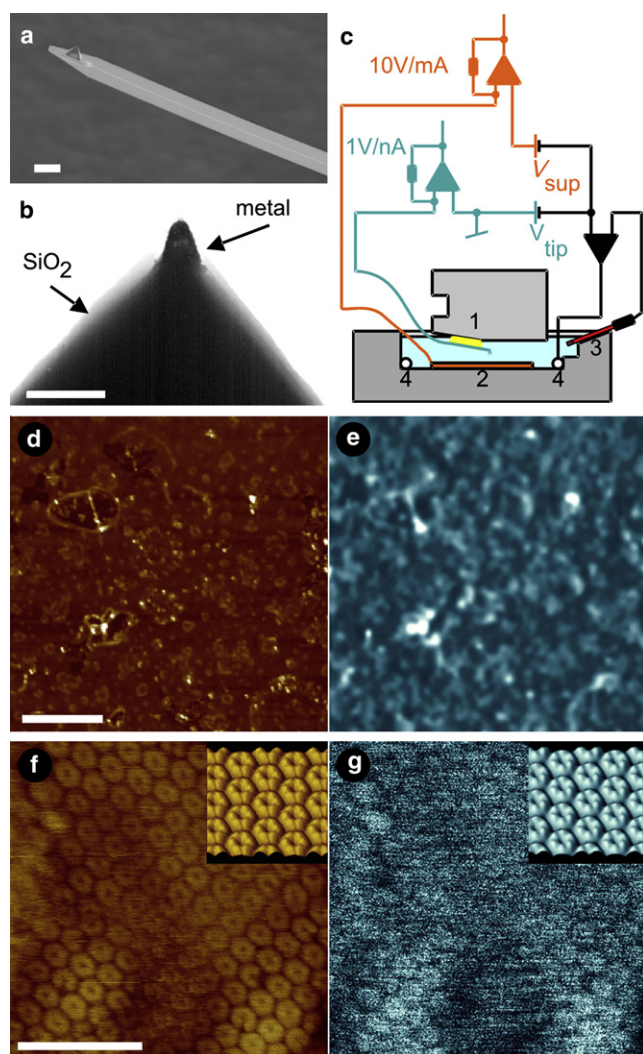
FIGURE 2 Combined atomic force and scanning electrochemical microscopy (AFM-SECM). (*a*) Scanning electron micrograph of an insulated, conductive cantilever. The metal lead contacting the tip electrode is visible as the narrow, light stripe in the cantilever. (*b*) Transmission electron micrograph at higher magnification of the cantilever tip, showing the metal electrode sticking out of the insulating layer of SiO_2. (*c*) Schematic overview of a AFM-SECM setup, using a bipotentiostat to independently apply voltages to cantilever electrode (1) and support (2). Voltages are set against a reference electrode (3). A counter electrode (4) supplies the current flowing through cantilever and support. (*d*) Topography and (*e*) current of a glucose-oxidase-modified graphite electrode in the presence of 10mM glucose. The cantilever electrode detects H_2O_2 released during the enzymatic reaction. No current was detected in absence of glucose. Adjusted from Kueng et al. (42). (*f*) Topography and (*g*) current of a tip scanning over hexagonally packed intermediate layer. The current reductions are caused by reduced accessibility of the tip to reactants when the tip enters a cleft. Adjusted from Frederix et al. (44). Scale bars *a*: 10 μm, *b*: 200 nm, *d, e*: 5 μm, *f* and *g*: 100nm; height range: *d*: 50nm, *f*: 10nm; current range: *e*: 2nA, *g*: 4pA).

(42,43) as illustrated in (Fig. 2, *d–e*). To study the relation between topography and function of single membrane proteins, conductive probes should provide a resolution of a few nm. Using batch-fabricated conductive cantilevers,

hexagonally packed intermediate layer (Fig. 2 *f*) and the outer membrane protein, OmpF (Fig. 3 *d*) were imaged at a resolution similar to that of conventional AFM probes (44,45). Further improvements may result from nano-wires attached at the end of a conductive cantilever (46). For implementation of AFM-SECM the AFM must be extended with a (bi)potentiostat that can reliably apply a voltage to the cantilever electrode and, if applicable, to a conductive support or sample (Fig. 2 *c*). An emerging new application is the local probing of the surface topography of channel proteins in combination with diffusion of redox molecules through them. To this end, flat, conductive supports are required that can swiftly transfer electrons from or to redox molecules. Recent experiments have shown that template stripped gold and platinum electrodes serve this purpose best (45).

Sample preparation and imaging

Detailed, step-by-step protocols for preparing biological membranes and for AFM imaging have been provided (5). In general, membranes are adsorbed to a chemically inert hydrophilic and flat solid support by properly adjusting pH and ionic strength. Such solid-supported membranes have allowed, and will still allow, important insights to be gained into the structure and function relationship of native membrane proteins. Solid supports that have proven suitable for high-resolution imaging of membrane proteins include mica (47), highly oriented pyrolitic graphite (33,45,48), molybdenum disulfide (45), template stripped gold (45,49), and template stripped platinum (45). Template stripped metal surfaces appear to be particularly useful for combined topographical and electronic measurements (45) (Fig. 3).

Although high-resolution imaging is possible exclusively on solid-supported membranes, certain questions may not be addressed by this preparation method. For example, membrane proteins in membranes directly attached to the support often exhibit impaired mobility (50–52), because the gap between membrane and support is only 0.5–2 nm. Moreover, adsorption forces may influence the conformation of membrane proteins, and it is known that lipids of a solid-supported lipid bilayer can show different structural features than the lipids of a vesicle or a free-standing lipid bilayer (52). Various schemes have been proposed to circumvent this problem by using spacers that warrant a larger gap, or polymer cushions (53). Free-standing bacterial S-layers spanned over small wells have been imaged at high resolution in the AFM (54), representing an ideal situation. However, this still needs to be shown for proteins embedded in a free-standing lipid bilayer. Therefore, there is room for further progress in sample preparation strategies to study structure and function of native membrane protein assemblies by AFM.

Clean tips, contamination-free membrane surfaces and balanced electrostatic interactions are prerequisites for the acquisition of high-resolution topographs. Therefore, once the sample is properly immobilized on the support, and the
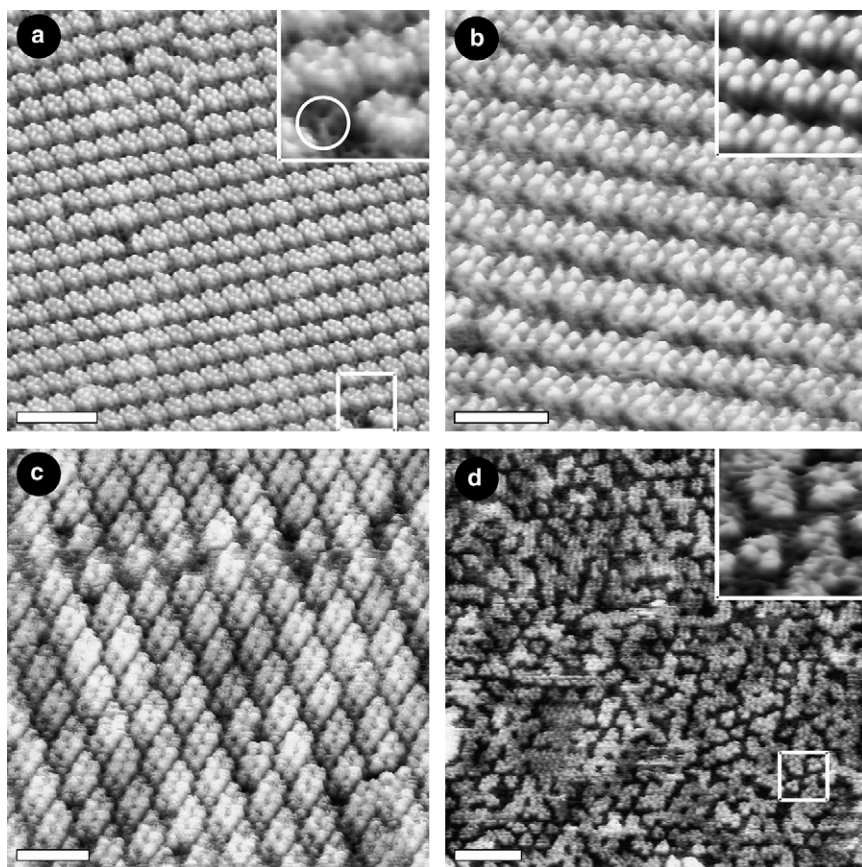
FIGURE 3 High resolution imaging of outer membrane protein OmpF 2D crystals adsorbed to different supports. OmpF reconstituted in the presence of DOPC assembled into orthogonal lattice with alternating rows of trimers facing up with their extracellular or periplasmic side. (*a*) on mica, (*b*) on MoS_2, (*c*) on template stripped gold and (*d*) on template stripped platinum. Metal surface are less flat than mica and MoS_2. Topograph (*d*) has been acquired with a conductive tip, all other images were taken with normal silicon nitride cantilevers. The image in *c* has a double tip artifact, resulting in eight instead of six protrusions for the extracellular side of two adjacent trimers. The inset in *a* shows the pore openings of an OmpF trimer from its periplasmic side. The inset in *b* is the twofold symmetrized correlation average of topograph *b*. The inset in *d* reveals well resolved trimers. Reconstituted OmpF 2D crystals adsorbed on gold or platinum generally lie less flat than on mica, highly oriented graphite or MoS_2, as revealed by distinct height variations extending laterally over a few unit cells (*c* and *d*). Images are low pass filtered over 1–2 pixels to reduce noise and image *d* was high pass filtered to reduce low frequency height variations in the patch. Images are 3D projections, rotated over 3–5 degrees. Scale bars *a* and *d*: 50 nm; *b* and *c*: 25 nm; height range: *a* and *d*: 3 nm, *b* and *c*: 2 nm, side length of all insets: 36 nm.

AFM is thermally equilibrated, force-distance curves should be recorded before even scanning the sample at low magnification and low scan speed (5). Force measurements are repeated on suitable membrane patches, and buffer conditions may be adapted to achieve the best possible resolution (55). This straightforward protocol has allowed lateral resolutions of 0.5–1 nm to be routinely achieved on relatively flat and clean 2D crystals of membrane proteins (Fig. 4). It exploits the possibility to tune pH and ionic strength in a way to achieve an appropriate electrostatic repulsion of the silicon nitride tip by a negatively charged sample surface.

Image processing

As result of the high signal/noise ratio, meaningful substructures can be directly discerned in high-resolution images of single proteins. Nevertheless, line-by-line background correction is applied routinely to most images acquired by AFM, as well as low-pass filtering for enhancing the visibility of single proteins. Such simple processing can be done by software provided by the microscope manufacturers. Calculation of averages from many images of individual proteins using methods and program packages developed for electron microscopy may further enhance details in topographs. To assess the lateral resolution of AFM images the autocorrelation signal has been used. For 2D crystals the power spectrum allows the diffraction spots to be indexed, and the highest diffraction spots

to be identified. In addition, crystallographic averaging methods used in electron microscopy may be applied. Such image processing methods do not extract all the pertinent information of a high-resolution topograph, but it may rather dilute it. Since peptide loops of individual membrane proteins are resolved, simple averaging is not required. In an early attempt to extract more information than an average, the standard deviation was calculated to identify flexible regions (56). Alternatively, the positions of protrusions related to loops connecting transmembrane α-helices were determined for an ensemble of single membrane proteins and represented as a position probability map. The Boltzmann law relates such maps directly to the surface energy landscape, which provides a quantitative measure for assessing the surface dynamics of membrane proteins (57) (Fig. 4, *e* and *f*).

Imaging native membranes

The AFM is currently the only microscope that allows images of native membranes to be acquired at submolecular resolution. In most other methods available today to analyze membrane proteins at high resolution, the protein needs to be solubilized, purified, and further processed to be amenable to analysis. Therefore, the AFM provided new insights into the native organization of membrane proteins and their complexes. Disk membranes prepared from mouse retina and deposited on mica could be imaged by AFM at sufficient
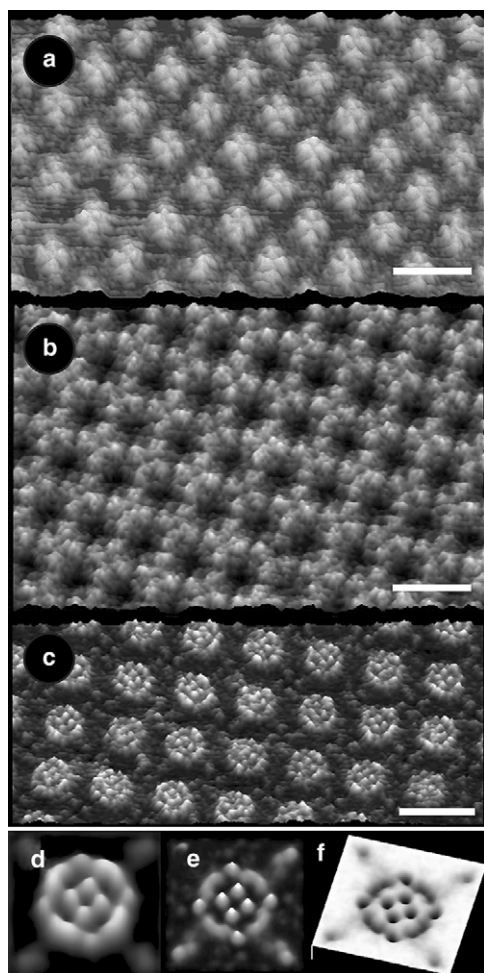
FIGURE 4 Surface topographies of aquaporins. These highly specific pores for water mediate water homeostasis in all organisms and exhibit a highly conserved pore structure. In contrast, loops connecting the six transmembrane helices are not conserved and adopt different conformations, as demonstrated by striking differences in the surface topography of (*a*) human AQP1, (*b*) human AQP2, and (*c*) bacterial AqpZ. In addition to variation of the surface structure, these tetrameric proteins exhibit different packing arrangements when reconstituted into 2D crystals in the presence of lipids. Nevertheless, the prominent protrusions result from extraclellular loops in all forms displayed. Image processing allows the average surface topography to be elucidated (*d*). Of particular interest is the map of the probability to observe specific loops at specific sites in the unit cell (*e*). This map reflects the mobility of a loop or feature and can be translated into the surface energy landscape using Boltzmann's law (57). Scale bars *a–c*: 10 nm; width of frames *d–f*: 9.5 nm; height range: *a–c*: 1 nm.

resolution to identify the native packing arrangement of rhodopsin (58). Rhopdopsins were found to pack in rows of dimers (Fig. 5 *a*), which provide a platform for interaction with arrestin as well as transducin. Although these topographs provided compelling evidence for the existence of rhodopsin dimers and higher oligomers, the controversial issue whether G-protein coupled receptors are generally active as a monomer or as a higher oligomer is not resolved.
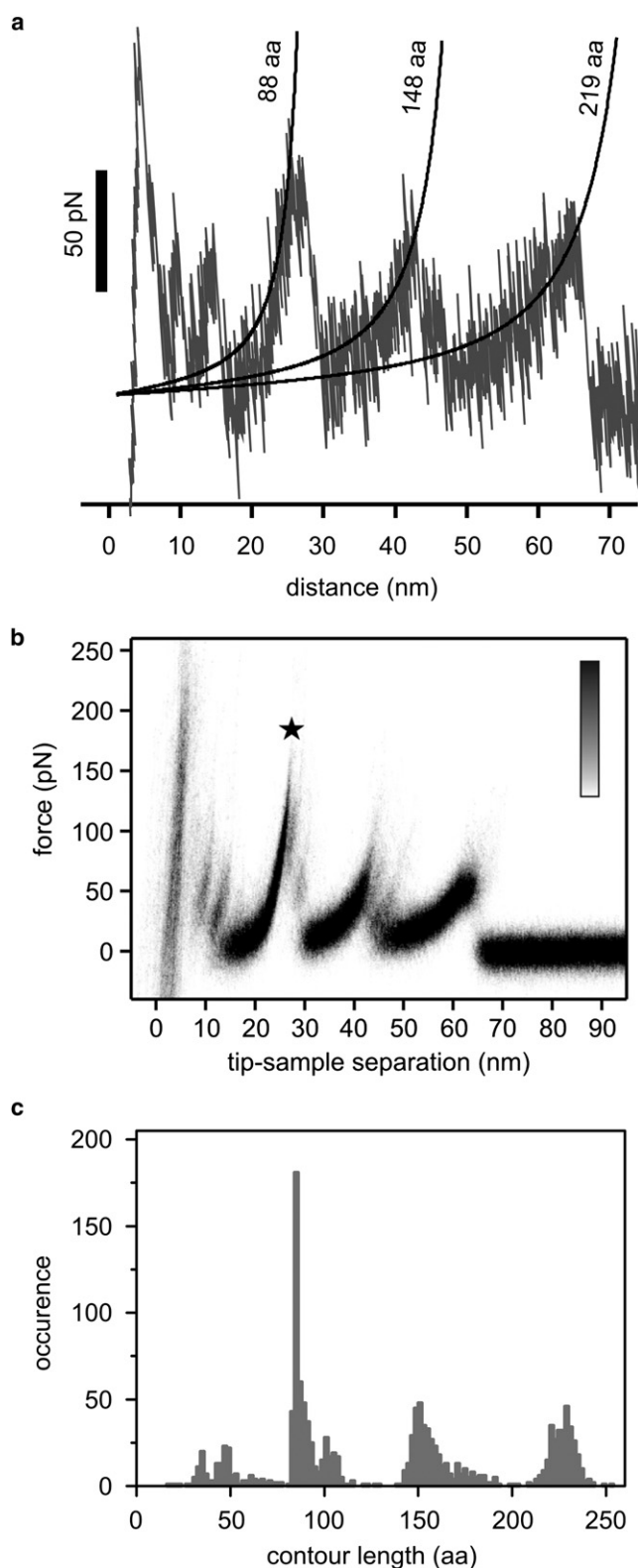
Topographs of native membranes from different photosynthetic bacteria acquired by AFM have provided new
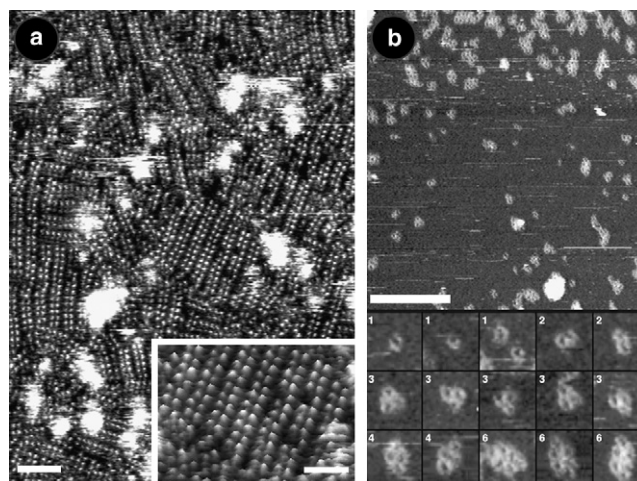
FIGURE 5 Topographs of native membranes. (*a*) Murine disc membranes revealing the tight packing of native rhodopsin. Most of the rhodopsins are arranged as dimers that form extended rows. Single rhodopsins are unfrequent. Dimeric packing is likely to be important for signal transduction (58). (*b*) Outer mitochondrial membranes reveal VDACs in different oligomeric states (20). The use of the frequency-modulated dynamic-imaging mode (18) allowed topographs of single VDACs to be recorded. Scale bars *a*: 10 nm, inset: 5 nm, in *b*: 75 nm. Boxes in *b* have a side length of 21 nm. Height range: *a*: 1.6 nm, *b*: 2.3 nm.

information on the architecture of the photosynthetic apparatus (reviewed in (59)). These membranes have been imaged at sufficient resolution to visualize individual subunits. Such images have also revealed the structural changes of the photosynthetic machinery during chromatic adaptation of *R. photometricum* to high-light and low-light growth conditions (60). An insightful atomic model of the light-harvesting system has subsequently been established by using the surface topography acquired by AFM and the atomic structures of individual subunits.

Outer mitochondrial membranes house specific proteins that ensure metabolic coupling and signaling between the cytosol and mitochondria. A major gateway for the molecular traffic is the VDAC, a general diffusion pore exhibiting a diameter of 2–3 nm. VDACs have a molecular mass of ~30 kDa per channel, and have been shown to reduce their conductance at membrane potentials $> |20mV|$. Although electron microscopy has revealed these pores in 2D crystals induced by treatment of outer mitochondrial membranes with phospholipase A2 (62), their native organization has been elusive. Only recently has it been possible to directly image these channels in native outer membranes of mitochondria from potato (20) and from yeast (61). In some membrane domains, VDACs were found to be packed at high density like bacterial outer membrane porins (61), whereas in other domains VDACs were loosely packed, exhibiting single pores and oligomeric clusters comprising two, three, four, and six channels (20) (Fig. 5 *b*). Frequency-modulated AFM mode yielded the best images of VDACs, in particular of single pores that were not visualized by contact mode, probably as result of lateral friction forces.

The tight stacking of fiber cells is a prerequisite for lens transparency and is mediated by thin junctions formed by lens-specific aquaporin 0 (AQP0) that conducts water and is involved in cell adhesion. These thin junctions coexist with gap junctions formed by connexons, which allow ions and metabolites to pass between cells. High-resolution AFM images revealed the supramolecular organization of these proteins in native lens core membranes, in which AQP0 forms two-dimensional arrays that are surrounded by densely packed gap junction channels (4,63). The images also showed that the conformation of the extracellular loops of these AQP0 molecules closely resembles that of junctional AQP0 of the lens core, in which the water pore is thought to be closed.

Single molecule force spectroscopy

The capability of the AFM to measure pN forces has stimulated its application to study forces between cells and components of supramolecular assemblies, as well as intramolecular forces stabilizing the fold of a protein (64–66). Whereas van der Waals attraction tethers the membranes to a solid support like mica, a terminus or a loop of the single membrane proteins is either physisorbed to the tip by enhanced contact forces, or covalently attached to the gold coated tip via a surface exposed cystein (67). Upon retraction of the tip the single memebrane protein is then unfolded. Imaging a purple membrane or bacterial S-layers at high resolution allowed individual proteins to be addressed, contacted and unfolded, and the vacancy produced to be imaged (67–69).

Stable structural segments, which can be represented by grouped, single or parts of secondary structure elements, build unfolding barriers that stabilize the membrane protein (70), and that can be represented in their full complexity by the potential energy landscape (66, 71). During unfolding the external force is transmitted through the already unfolded backbone of the protein and acts together with thermal fluctuations to overcome barriers. Since thermal fluctuations are random events with extreme peaks occurring with low probability, the force required to overcome the barrier will depend on the rate at which the force is increased (72,73).

Since proteins are picked up at random positions of the protein surface, only force-distance curves showing the full length of the unfolded protein are selected for a comparative analysis. For each barrier conquered a further segment is released and increases the length of the unfolded polypeptide transmitting the force to the next barrier, and the force collapses. As the tip retracts further, the force increases again until the next barrier breaks. Each force peak can be fitted using the worm-like chain model with a single free parameter:

FIGURE 6 Force spectroscopy of membrane proteins. Bacteriorhodopsin molecules were pulled out of their membrane, using a semiautomated force spectroscopy protocol (77). (*a*) Exemplary curve, showing force against tip-sample separation. At barriers in the sequence, a certain force is required to unfold a part of the protein up to the next barrier. The smooth lines are fitted curves using a worm like chain model to describe force again polymer length. (*b*) Scattering plot comprising 398 full-length force-distance curves. Force spectra were aligned with respect to the unfolding peak denoted by star. (*c*) Histogram, showing fitted contour length values from 398 unfolded molecules as detailed in Puchner et al. (75).

the contour length of the unfolded polypeptide (74) (Fig. 6 *a*). Accumulation of length values in the contour length histogram provides a convenient representation of the data (75) (Fig. 6 *c*). The histogram relates barriers to the primary sequence and allows them to be mapped on the structure of the membrane protein. In general, unfolding force peaks, and thus the apparent barrier heights, decrease as unfolding progresses because parts of the protein have already been extracted. Nonspecific interactions between the tip and sample usually prevent assessment of specific interaction during the first few nanometers of the unfolding trace.

It is possible to compare the barriers observed for unfolding from the N-terminus with those from the C terminus. The barrier positions and heights found in bacteriorhodopsin when probed from both sides were located not only in or at the ends of stiff α-helical rods, but also in loops that are not well resolved in structural investigations (76). Certain barrier positions were found to coincide with each other when probed from both sides. These barriers must be stabilized in both directions, upstream and downstream, i.e., by structural elements of similar strength irrespective of what part of the protein has already been extracted from the membrane. Two forms of L-arginine/agmatine antiporter AdiC (N-His6-AdiC and AdiC-His6-C) have been expressed, purified and reconstituted into densely packed proteoliposomes to facilitate such force measurements. The data acquired by a highly automated protocol suggest a possible packing arrangement of specific helical bundles (77).

An interesting application of single molecule force spectroscopy of membrane proteins is the localization of ligand binding sites. Barriers may not only be signatures of the intramolecular bonds, but they may also reflect the interaction of ligands with the protein. The feasibility of localizing such barriers with the precision of a few amino acids and to determine the binding energy has recently been demonstrated (78). Single molecule force spectroscopy has also been combined with imaging, in that force measurements have been done in a raster-scanned manner, mapping the forces measured to particular locations on the specimen scanned (79). For example, *trans*-membrane Na^+/D-glucose cotransporters were mapped on brush border membranes using phlorizin, a competitive high affinity inhibitor, as ligand on the AFM tip (80).

CONCLUSION

Since its invention more than two decades ago, the AFM has become an important tool for structural biologists. It is the only instrument that allows surfaces of cells, supramolecular assemblies and single molecules to be imaged in the native aqueous environment at nanometer-scale resolution. In addition, it makes manipulation of such structures at this scale possible. Recent developments of cantilevers, deflection sensors, imaging modes, and fast scan systems demonstrate the potential possibilities to improve the AFM. Such progress will enhance the applicability of AFM to a wider range of biological questions, and will allow data to be acquired more efficiently than previously possible. AFM images of native membranes at submolecular resolution have provided a wealth of novel insights, and it is likely that this particular application of AFM will yield further important results. Measurements of forces between cells, within supramolecular aggregates, or forces dictating the fold of proteins can now be executed with great efficiency allowing large data sets to be acquired, delivering quantitative information previously not accessible. As instrumentation development progresses, sample preparation methods have to be improved as well. There is room for improving the immobilization of native biological membranes to make them accessible to high-resolution imaging and manipulation with the AFM. The rapid progress over the past few years suggests that the AFM will deliver substantial new information about the structure, dynamics and function of diverse native biological membranes.

REFERENCES

1. Binnig, G., C. F. Quate, and C. Gerber. 1986. Atomic force microscope. *Phys. Rev. Lett.* 56:930–933.

2. Drake, B., C. B. Prater, A. L. Weisenhorn, S. A. Gould, T. R. Albrecht, et al. 1989. Imaging crystals, polymers and processes in water with the atomic force microscope. *Science*. 243:1586–1589.

3. Hoh, J. H., R. Lal, S. A. John, J. P. Revel, and M. F. Arnsdorf. 1991. Atomic force microscopy and dissection of gap junctions. *Science*. 253:1405–1408.

4. Buzhynskyy, N., R. K. Hite, T. Walz, and S. Scheuring. 2007. The supramolecular architecture of junctional microdomains in native lens membranes. *EMBO Rep*. 8:51–55.

5. Muller, D. J., and A. Engel. 2007. Atomic force microscopy and spectroscopy of native membrane proteins. *Nat. Protocols*. 2:2191–2197.

6. Czajkowsky, D. M., E. M. Hotze, Z. Shao, and R. K. Tweten. 2004. Vertical collapse of a cytolysin prepore moves its transmembrane beta-hairpins to the membrane. *EMBO J*. 23:3206–3215.

7. Fotiadis, D., P. Qian, A. Philippsen, P. A. Bullough, A. Engel, et al. 2004. Structural Analysis of the Reaction Center Light-harvesting Complex I Photosynthetic Core Complex of Rhodospirillum rubrum Using Atomic Force Microscopy. *J. Biol. Chem*. 279:2063–2068.

8. Kienberger, F., H. Mueller, V. Pastushenko, and P. Hinterdorfer. 2004. Following single antibody binding to purple membranes in real time. *EMBO Rep*. 5:579–583.

9. Muller, D. J., G. M. Hand, A. Engel, and G. E. Sosinsky. 2002. Conformational changes in surface structures of isolated connexin 26 gap junctions. *EMBO J*. 21:3598–3607.

10. Sader, J. E. 1998. Frequency response of cantilever beams immersed in viscous fluids with applications to the atomic force microscope. *J. Appl. Phys*. 84:64–76.

11. Yasumura, K. Y., T. D. Stowe, E. M. Chow, T. Pfafman, T. W. Kenny, et al. 2000. Quality factors in micron- and submicron-thick cantilevers. *J. Microelectromech. Syst.* 9:117–125.

12. Fukuma, T., and S. Jarvis. 2006. Development of liquid-environment frequency modulation atomic force microscope with low noise deflection sensor for cantilevers of various dimensions. *Rev. Sci. Instrum.* 77:043701–043708.

13. Hoogenboom, B. W., P. L. T. M. Frederix, J. Yang, S. Martin, Y. Pellmont, et al. 2005. A Fabry-Perot interferometer for micrometer-sized cantilevers. *Appl. Phys. Lett.* 86:074101.

14. Hoogenboom, B. W., P. L. T. M. Frederix, D. Fotiadis, H. J. Hug, and A. Engel. 2008. Potential of interferometric cantilever detection and its application for SFM/AFM in liquids. *Nanotechnology.* 19:384013–384024.

15. Ashby, P. D. 2007. Gentle imaging of soft materials in solution with amplitude modulation atomic force microscopy: Q control and thermal noise. *Appl. Phys. Lett.* 91:254102.

16. Fukuma, T., M. J. Higgins, and S. P. Jarvis. 2007. Direct imaging of individual intrinsic hydration layers on lipid bilayers at Angstrom resolution. *Biophys. J.* 92:3603–3609.

17. Uchihashi, T., M. J. Higgins, S. Yasuda, S. P. Jarvis, S. Akita, et al. 2004. Quantitative force measurements in liquid using frequency modulation atomic force microscopy. *Appl. Phys. Lett.* 85:3575–3577.

18. Hoogenboom, B. W., H. J. Hug, Y. Pellmont, S. Martin, P. L. T. M. Frederix, et al. 2006. Quantitative dynamic-mode scanning force microscopy in liquid. *Appl. Phys. Lett.* 88:193109.

19. Fukuma, T., K. Kobayashi, K. Matsushige, and H. Yamada. 2005. True atomic resolution in liquid by frequency-modulation atomic force microscopy. *Appl. Phys. Lett.* 87:034101.

20. Hoogenboom, B. W., K. Suda, A. Engel, and D. Fotiadis. 2007. The supramolecular assemblies of voltage-dependent anion channels in the native membrane. *J. Mol. Biol.* 370:246–255.

21. Tamayo, J., A. D. Humphris, R. J. Owen, and M. J. Miles. 2001. High-Q dynamic force microscopy in liquid and its application to living cells. *Biophys. J.* 81:526–537.

22. Han, W. H., S. M. Lindsay, and T. W. Jing. 1996. A magnetically driven oscillating probe microscope for operation in liquids. *Appl. Phys. Lett.* 69:4111–4113.

23. Stark, R. 2004. Spectroscopy of higher harmonics in dynamic atomic force microscopy. *Nanotechnology.* 15:347–351.

24. Sahin, O., S. Magonov, C. Su, C. F. Quate, and O. Solgaard. 2007. An atomic force microscope tip designed to measure time-varying nanomechanical forces. *Nat. Nanotechnol.* 2:507–514.

25. Viani, M. B., T. E. Schäffer, G. T. Paloczi, L. I. Pietrasanta, B. L. Smith, et al. 1999. Fast imaging and fast force spectroscopy of single biopolymers with a new atomic force microscope designed for small cantilevers. *Rev. Sci. Instrum.* 70:4300–4303.

26. Picco, L. M., L. Bozec, A. Ulcinas, D. J. Engledew, M. Antognozzi, et al. 2007. Breaking the speed limit with atomic force microscopy. *Nanotechnology.* 18:44030–44033.

27. Ando, T., T. Uchihashi, N. Uchihashi, D. Yamamoto, A. Miyagi, et al. 2008. High-speed AFM and nano-visualization of biomolecular processes. *Pflug. Arch. Eur. J. Phy.* 456:211–225.

28. Yokokawa, M., C. Wada, T. Ando, N. Sakai, A. Yagi, et al. 2006. Fast-scanning atomic force microscopy reveals the ATP/ADP-dependent conformational changes of GroEL. *EMBO J.* 25:4567–4576.

29. Müller, D. J., G. Büldt, and A. Engel. 1995. Force-induced conformational change of bacteriorhodopsin. *J. Mol. Biol.* 249:239–243.

30. Scheuring, S., P. Ringler, M. Borgnia, H. Stahlberg, D. J. Muller, et al. 1999. High resolution AFM topographs of the Escherichia coli water channel aquaporin Z. *EMBO J.* 18:4981–4987.

31. Engel, A. and D. J. Muller. 2000. Observing single biomolecules at work with the atomic force microscope. *Nat. Struct. Biol.* 7:715–718.

32. Fisher, T. E., P. E. Marszalek, and J. M. Fernandez. 2000. Stretching single molecules into novel conformations using the atomic force microscope. *Nat. Struct. Biol.* 7:719–724.

33. Muller, D. J., and A. Engel. 1999. Voltage and pH-induced channel closure of porin OmpF visualized by atomic force microscopy. *J. Mol. Biol.* 285:1347–1351.

34. Andersen, C., B. Schiffler, A. Charbit, and R. Benz. 2002. PH-induced collapse of the extracellular loops closes Escherichia coli maltoporin and allows the study of asymmetric sugar binding. *J. Biol. Chem.* 277:41318–41325.

35. Unwin, N., A. Miyazawa, J. Li, and Y. Fujiyoshi. 2002. Activation of the nicotinic acetylcholine receptor involves a switch in conformation of the alpha subunits. *J. Mol. Biol.* 319:1165–1176.

36. Hilge, M., G. Siegal, G. W. Vuister, P. Guntert, S. M. Gloor, et al. 2003. ATP-induced conformational changes of the nucleotide-binding domain of Na, K-ATPase. *Nat. Struct. Biol.* 10:468–474.

37. Subramaniam, S., and R. Henderson. 2000. Molecular mechanism of vectorial proton translocation by bacteriorhodopsin. *Nature.* 406:653–657.

38. Grabiec, P., T. Gotszalkb, J. Radojewskib, K. Edingerc, N. Abedinovd, et al. 2002. SNOM/AFM microprobe integrated with piezoresistive cantilever beam for multifunctional surface analysis. *Microelectron. Eng.* 61–62:981–986.

39. Hansma, P. K., B. Drake, O. Marti, S. A. Gould, and C. B. Prater. 1989. The scanning ion-conductance microscope. *Science.* 243:641–643.

40. Gardner, C. E., and J. V. Macpherson. 2002. Atomic force microscopy probes go electrochemical. *Anal. Chem.* 74:576A–584A.

41. Kranz, C., and J. Wiedemair. 2008. Scanning force microscopy based amperometric biosensors. *Anal. Bioanal. Chem.* 390:239–243.

42. Kueng, A., C. Kranz, A. Lugstein, E. Bertagnolli, and B. Mizaikoff. 2003. Integrated AFM-SECM in tapping mode: simultaneous topographical and electrochemical imaging of enzyme activity. *Angew. Chem. Int. Ed. Engl.* 42:3238–3240.

43. Hirata, Y., S. Yabuki, and F. Mizutani. 2004. Application of integrated SECM ultra-micro-electrode and AFM force probe to biosensor surfaces. *Bioelectrochemistry.* 63:217–224.

44. Frederix, P. L. T. M., M. R. Gullo, T. Akiyama, A. Tonin, N. F. de Rooij, et al. 2005. Assessment of insulated conductive cantilevers for biology and electrochemistry. *Nanotechnology.* 16:997–1005.

45. Frederix, P. L. T. M., P. D. Bosshart, T. Akiyama, M. Chami, M. R. Gullo, et al. 2008. Conductive supports for combined AFM-SECM on biological membranes. *Nanotechnology.* 19:384004–384013.

46. Burt, D. P., N. R. Wilson, J. M. R. Weaver, P. S. Dobson, and J. V. Macpherson. 2005. Nanowire probes for high resolution combined scanning electrochemical Microscopy - Atomic force Microscopy. *Nano Lett.* 5:639–643.

47. Muller, D. J., M. Amrein, and A. Engel. 1997. Adsorption of biological molecules to a solid support for scanning probe microscopy. *J. Struct. Biol.* 119:172–188.

48. Scheuring, S., D. J. Muller, P. Ringler, J. B. Heymann, and A. Engel. 1999. Imaging streptavidin 2D crystals on biotinylated lipid monolayers at high resolution with the atomic force microscope. *J. Microsc.* 193:28–35.

49. Cisneros, D. A., D. J. Muller, S. M. Daud, and J. H. Lakey. 2006. An approach to prepare membrane proteins for single-molecule imaging. *Angew. Chem. Int. Ed.* 45:3252–3256.

50. Wagner, M. L. and L. K. Tamm. 2000. Tethered polymer-supported planar lipid bilayers for reconstitution of integral membrane proteins: silane-polyethyleneglycol-lipid as a cushion and covalent linker. *Biophys. J.* 79:1400–1414.

51. Müller, D. J., A. Engel, U. Matthey, T. Meier, P. Dimroth, et al. 2003. Observing membrane protein diffusion at subnanometer resolution. *J. Mol. Biol.* 327:925–930.

52. Tanaka, M., and E. Sackmann. 2005. Polymer-supported membranes as models of the cell surface. *Nature.* 437:656–663.

53. Müller, D., and A. Engel. 2008. Strategies to prepare and characterize native membrane proteins and protein membranes by AFM. *Curr. Opin. Colloid Interface Sci.* 13:338–350.

54. Goncalves, R. P., G. Agnus, P. Sens, C. Houssin, B. Bartenlian, et al. 2006. Two-chamber AFM: probing membrane proteins separating two aqueous compartments. *Nat. Methods.* 3:1007–1012.

55. Muller, D. J., D. Fotiadis, S. Scheuring, S. A. Muller, and A. Engel. 1999. Electrostatically balanced subnanometer imaging of biological specimens by atomic force microscope. *Biophys. J.* 76:1101–1111.

56. Muller, D. J., D. Fotiadis, and A. Engel. 1998. Mapping flexible protein domains at subnanometer resolution with the atomic force microscope. *FEBS Lett.* 430:105–111.

57. Scheuring, S., D. J. Muller, H. Stahlberg, H. A. Engel, and A. Engel. 2002. Sampling the conformational space of membrane protein surfaces with the AFM. *Eur. Biophys. J.* 31:172–178.

58. Fotiadis, D., Y. Liang, S. Filipek, D. A. Saperstein, A. Engel, et al. 2003. Atomic-force microscopy: Rhodopsin dimers in native disc membranes. *Nature.* 421:127–128.

59. Scheuring, S. 2006. AFM studies of the supramolecular assembly of bacterial photosynthetic core-complexes. *Curr. Opin. Chem. Biol.* 10:387–393.

60. Scheuring, S., and J. N. Sturgis. 2005. Chromatic adaptation of photosynthetic membranes. *Science.* 309:484–487.

61. Goncalves, R. P., N. Buzhynskyy, V. Prima, J. N. Sturgis, and S. Scheuring. 2007. Supramolecular assembly of VDAC in native mitochondrial outer membranes. *J. Mol. Biol.* 369:413–418.

62. Mannella, C. A. 1984. Phospholipase-induced crystallization of channels in mitochondrial outer membranes. *Science.* 224:165–166.

63. Scheuring, S., N. Buzhynskyy, S. Jaroslawski, R. P. Goncalves, R. K. Hite, et al. 2007. Structural models of the supramolecular organization of AQP0 and connexons in junctional microdomains. *J. Struct. Biol.* 160:385–394.

64. Gamsjaeger, R., A. Johs, A. Gries, H. J. Gruber, C. Romanin, et al. 2005. Membrane binding of beta2-glycoprotein I can be described by a two-state reaction model: an atomic force microscopy and surface plasmon resonance study. *Biochem. J.* 389:665–673.

65. Baumgartner, W., P. Hinterdorfer, W. Ness, A. Raab, D. Vestweber, et al. 2000. Cadherin interaction probed by atomic force microscopy. *Proc. Natl. Acad. Sci. USA.* 97:4005–4010.

66. Clausen-Schaumann, H., M. Seitz, R. Krautbauer, and H. E. Gaub. 2000. Force spectroscopy with single bio-molecules. *Curr. Opin. Chem. Biol.* 4:524–530.

67. Oesterhelt, F., D. Oesterhelt, M. Pfeiffer, A. Engel, H. E. Gaub, et al. 2000. Unfolding pathways of individual bacteriorhodopsins. *Science.* 288:143–146.

68. Müller, D. J., W. Baumeister, and A. Engel. 1999. Controlled unzipping of a bacterial surface layer with atomic force microscopy. *Proc. Natl. Acad. Sci. USA.* 96:13170–13174.

69. Scheuring, S., H. Stahlberg, M. Chami, C. Houssin, J. L. Rigaud, et al. 2002. Charting and unzipping the surface layer of Corynebacterium glutamicum with the atomic force microscope. *Mol. Microbiol.* 44:675–684.

70. Sapra, K. T., H. Besir, D. Oesterhelt, and D. J. Muller. 2006. Characterizing molecular interactions in different bacteriorhodopsin assemblies by single-molecule force spectroscopy. *J. Mol. Biol.* 355:640–650.

71. Preiner, J., H. Janovjak, C. Rankl, H. Knaus, D. A. Cisneros, et al. 2007. Free energy of membrane protein unfolding derived from single-molecule force measurements. *Biophys. J.* 93:930–937.

72. Evans, E., and F. Ludwig. 1999. Dynamic strength of molecular anchoring and material cohesion in fluid biomembranes. *J. Phys. Condens. Matter.* 11:1–6.

73. Evans, E. 2001. Probing the relation between force–lifetime–and chemistry in single molecular bonds. *Annu. Rev. Biophys. Biomol. Struct.* 30:105–128.

74. Kellermayer, M. S., S. B. Smith, H. L. Granzier, and C. Bustamante. 1997. Folding-unfolding transitions in single titin molecules characterized with laser tweezers. *Science.* 276:1112–1116.

75. Puchner, E. M., G. Franzen, M. Gautel, and H. E. Gaub. 2008. Comparing proteins by their unfolding pattern. *Biophys. J.* 95:426–434.

76. Kessler, M., and H. E. Gaub. 2006. Unfolding barriers in bacteriorhodopsin probed from the cytoplasmic and the extracellular side by AFM. *Structure.* 14:521–527.

77. Bosshart, P., F. Casagrande, P. Frederix, M. Ratera, V. Bippes, et al. 2008. High-throughput single molecule force spectroscopy for membrane proteins. *Nanotechnology.* 19:384014–384028.

78. Kedrov, A., M. Krieg, C. Ziegler, W. Kuhlbrandt, and D. J. Muller. 2005. Locating ligand binding and activation of a single antiporter. *EMBO Rep.* 6:668–674.

79. Stroh, C. M., A. Ebner, M. Geretschlager, G. Freudenthaler, F. Kienberger, et al. 2004. Simultaneous topography and recognition imaging using force microscopy. *Biophys. J.* 87:1981–1990.

80. Wielert-Badt, S., P. Hinterdorfer, H. J. Gruber, J. T. Lin, D. Badt, et al. 2002. Single molecule recognition of protein binding epitopes in brush border membranes by force microscopy. *Biophys. J.* 82:2767–2774.